Results in Engineering 22 (2024) 102010

Contents lists available at ScienceDirect

Results in Engineering

journal homepage: www.sciencedirect.com/journal/results-in-engineering

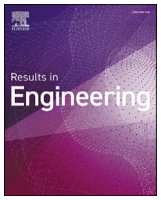

Research paper

Rain erosion atlas for wind turbine blades based on ERA5 and NORA3 for Scandinavia

Ásta Hannesdóttir [a], Stephan T. Kral [b,*], Joachim Reuder [b], Charlotte Bay Hasager [a,b]

[a] Department of Wind and Energy Systems, Technical University of Denmark, Frederiksborgvej 399, 4000, Roskilde, Denmark
[b] Geophysical Institute and Bergen Offshore Wind Centre, University of Bergen and Bjerknes Centre for Climate Research, Allegaten 70, N-5007, Bergen, Norway

ARTICLE INFO

Keywords:
Rain erosion atlas
Wind turbine blade coating
Precipitation and wind
Empirical damage model
Impingement to end of incubation
Offshore conditions

ABSTRACT

Leading edge erosion on wind turbine blades is a common issue, particularly for wind turbines placed in regions characterized by high wind speeds and precipitation. This study presents the development of a rain erosion atlas for Scandinavia and Finland, based on ERA5 reanalysis and NORA3 mesoscale model data on rainfall intensity and wind speed over five years. The IEA 15 MW reference wind turbine is used as an example to evaluate impingement water impact and erosion onset time for a commercial coating material. The damage progression is modeled by combining the wind speed and rainfall data with an empirical damage model that relates impinged water (H) as a function of impact velocity to the time of erosion onset. Comparative analyses at two weather station locations show that NORA3 data more accurately aligns with measurements in terms of power spectral density, mean wind speed, rainfall, and erosion prediction than ERA5. NORA3-based atlas layers offer finer spatial detail and predict shorter erosion onset times over land compared to ERA5, particularly in complex terrain. Conversely, the ERA5-based atlas suggests a shorter onset of erosion offshore. Based on NORA3 data, erosion onset time is estimated at 5 years on average for Baltic Sea wind farm sites and 3.2 years for sites in the North Sea.

1. Introduction

Leading edge erosion (LEE) at wind turbine blades is the damage of the surface of the blades due to environmental impacts [1,2], where rain is one of the dominant contributors. The cost for repair of blades due to erosion is considerable [3] and therefore there is a focus on understanding blade erosion, prevention, protection [4], and mapping the environmental factors leading to erosion and areas that have heightened risk of erosion [5] and damage progression.

Damage progression in blade coating materials are assessed in rain erosion tests following a recommended practice [6]. The tests involve high-speed rotation of blade material specimens on a whirling arm under needles dropping similar-sized droplets. Damage progression and lifetime predictions are based on factors like time, amount of water hitting the specimens, and impact speed. Recent advancements include droplet-size dependent lifetime prediction and comparisons between different testing methods [7].

The connecting links between rain erosion tests and real atmospheric conditions are 1) the speed of the specimen versus the tip speed of a turbine in operation, and 2) the droplet impact at the specimen in the rain erosion tester versus the multitude of droplets impact to the leading edge of the blades.

Studies on the relationship between atmospheric conditions and the risk of LEE have been explored. Some studies include observed damage at blades and atmospheric model rain data output for different climate zones in Europe [8–10]. Other studies include the prediction of blade lifetime based on local meteorological rain and wind observations from weather stations in Denmark [11], Germany [12], and the Netherlands [13,14]. Common to the studies based on local weather observations is that the results indicate a higher risk for erosion at coastal compared to inland sites. In the USA, a study based on weather radar data for a region in the Mid-West prone to severe hail show high LEE risk due to hail [15]. In Europe, hail prevails frequently in central and southern regions but lesser at high latitudes and offshore [16]. Satellite-based rain data used for the prediction of blade lifetime at sites in Denmark, Germany, and Portugal [17] yield lifetimes similar to those based on in situ rain data for most of the sites.

* Corresponding author.
E-mail address: stephan.kral@uib.no (S.T. Kral).

https://doi.org/10.1016/j.rineng.2024.102010
Received 5 January 2024; Received in revised form 7 March 2024; Accepted 8 March 2024
Available online 16 March 2024

In recent decades, numerous wind energy related atlases have been developed, ranging from regional to global scales. These atlases typically map the available wind resources [18–21] or siting parameters for wind turbines [22], aiding in project preparation and planning. They serve to identify areas of interest and potential risk prior to project initiation. However, despite the existence of these atlases, there remains a notable research gap concerning the mapping of rain erosion risk for wind turbine blades on a larger scale. To address this gap, we propose a methodology that integrates numerical simulations of environmental conditions with a rain erosion damage model. In this research we utilizes ERA5 [23], a global reanalysis model, and NORA3 [24], a mesoscale hindcasting model, to construct the first rain erosion atlas for Scandinavia.

The specific aim of the study is to provide the first rain erosion atlas for wind turbine blades covering Scandinavian and Finland based on numerical simulations of the environmental conditions and compare the simulation-based results to selected weather stations. The first objective is to assess the usability of ERA5 reanalysis data compared to NORA3 mesoscale model output for this specific purpose. ERA5 has the advantage of global coverage, while NORA3 has a superior spatial resolution making it a suitable candidate to investigate LEE in more complex terrain. First, a comparison of rain data from ERA5, NORA3, and two selected weather stations representing offshore conditions is performed. Second, an evaluation of the power spectra on wind speed and rainfall intensity for ERA5 and NORA3 versus weather station data is done to characterize the scales resolved by the models. Third, the turbine-specific information from one turbine types (IEA 15 MW) is combined with the spray mode VH-curve from the coating system tested in rain erosion test [7] and the results comprise an assessment of the impingement water and damage increments from ERA5, NORA3 and weather station data at two coastal sites. Finally, the rain erosion atlas using ERA5 and NORA3 is calculated for the IEA 15 MW turbine for the entire study area and the two resulting atlases are compared.

The second objective is to evaluate the results with a particular aim for offshore wind farm sites, where precipitation observations are sparse or non-existing. At the same time the risk of erosion is considerable at these sites.

The paper is structured as follows: Section 2 presents the data sources ERA5, NORA3, and weather station data and method using the damage model calculation for a reference wind turbine. Section 3 presents results starting with a comparison of the model and measurement data, including spectral analysis and statistical results for two measurement sites. Finally, the rain erosion atlases based on ERA5 and NORA3 are presented together with more detailed results for some existing or planned offshore sites. Section 4 contains the discussion and Section 5 conclusions.

2. Data and methodology

In this section, we describe the dataset used in the study and the methodology of the rain erosion calculation method.

2.1. Impingement model for damage calculations

The impingement of precipitation on turbine blades in operation causes gradual leading-edge erosion damage over time. The damage model we use in our study is based on rain erosion test data which is described in detail in Bech et al. [7]. The rain erosion tests are performed using a Rain Erosion Tester (RET) developed by R&D Test Systems A/S. This equipment contains a three-bladed rotor with one specimen per blade and can achieve rotor speeds of up to 1386 rpm. The rain field is created using needles that dispense water droplets of varying sizes and fall velocities, with the standard flow ensuring droplet formation by gravitational force and surface tension. During testing, images are taken at regular intervals to track erosion on the specimens. The collected data, after visual inspection analysis, depicts erosion as a function of time and position. The onset of visible erosion in the RET images indicates the initial failure of the protective coating. When this happens it is called the erosion onset time, or in other words, the incubation time. The damage typically starts near the high-velocity rotor tip and progresses inward. To quantify damage progression, the data is fitted to a power law function, called a VH curve, correlating the rotor velocity (V) to the impinged water column (H):

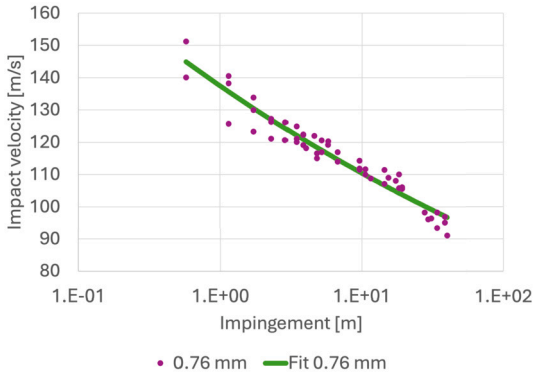

Fig. 1. Data points and fitted VH curve for end of incubation of the rain erosion test in spray mode.

$$H(V) = H_0 \left(\frac{V}{V_0} \right)^{-m} \tag{1}$$

where H_0 and m are parameters found from fitting the curve to data using the least-squares method and $V_0 = 1$ m/s is a normalization velocity.

Fig. 1 shows the RET data and fitted VH curve we use in our study. Each data point shows when the end of incubation is reached and erosion onset has started for a given impact velocity and impinged water. We can see from the figure that for an impact velocity of 110 m/s we will need 10 m of impinged water for erosion onset.

The fitted parameters we use in our study are $H_0 = 2.85 \times 10^{22}$ m and $m = 10.5$, which have been estimated from RET data where the needles were in spray mode, giving a broad distribution of droplet sizes (average droplet diameter of 76 mm) and fall velocities. The top coating that was used on the test specimens is a commercial polyurethane coating that is used on some modern wind turbine blades with relatively good erosion resistance.

2.2. Damage calculations from meteorological data

When using the impingement model with meteorological data, we need to convert measured or modeled rainfall data to impinged water on the blade tip by

$$h(U, I) = \frac{I}{V_{fall}(I)} V_{tip}(U) \Delta t \tag{2}$$

where I is the rainfall intensity in m/s, V_{fall} is the fall velocity of the rain droplets, V_{tip} is the tip speed of the wind turbine blade, Δt is the time step of the data in seconds, and U is the horizontal wind speed at hub height. This is done for every time step in the data time series. As the fall velocity of the rain droplets is not known in our study, it is derived from an empirical relation of droplet distribution and terminal velocities as a function of rainfall intensity [25]. The tip speed is found from a tip-speed curve as a function of wind speed at hub height. Here we use the IEA 15 MW reference wind turbine [26], which has a hub height of 150 m, blade length of 117 m, and maximum tip speed of 95 m/s (see more parameters in Table 1).

Damage calculations are based on the Palmgren-Miner rule [27], and an estimate of accumulated damage is obtained by

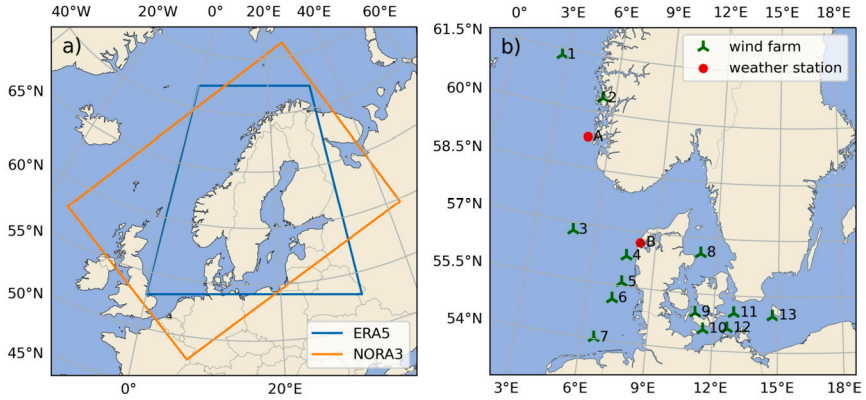

Fig. 2. a) A map of the selected domains of ERA5 data and NORA3 data. b) Locations of weather stations (red) and wind farms (green).

Table 1
The main parameters of the IEA 15 MW turbine.

IEA 15 MW	
Rotor diameter	240 m
Blade length	117 m
Cut-in wind speed	3 m/s
Rated wind speed	10.59 m/s
Cut-out wind speed	25 m/s
Minimum rotor speed	5 rpm
Maximum rotor speed	7.56 rpm
Minimum tip speed	62.83 m/s
Maximum tip speed	95 m/s
Hub height	150 m

$$D = \sum_{i=1}^{k} \frac{h_i(U_i, I_i)}{H_i(V_{rel})} \tag{3}$$

where k is the number of time steps and $V_{rel} = \sqrt{V_{tip}^2 + U^2}$ is the velocity of droplets relative to the blade.[1] The accumulated damage describes the onset of rain erosion when $D = 1$, i.e. the end of incubation and the initial failure of the coating due to liquid precipitation. Solid hydrometeors such as hail were not included in the RET and are therefore not taken into account by this modeling framework.

2.3. ERA5 reanalysis data

Wind speeds and precipitation from the "ERA5 hourly data on single levels from 1959 to present" provided by the European Union's Copernicus service are used. ERA5 is the fifth generation of the European Centre for Medium-Range Weather Forecast (ECMWF) atmospheric reanalysis of the global climate [23]. The dataset has an hourly temporal resolution and the spatial resolution is 0.25° which is equivalent to ~30 km horizontal resolution. We use the wind speed at 150 m (the hub height of the IEA 15 MW turbine) and total precipitation with a flag for liquid precipitation only. The ERA5 dataset has a spatial domain with global coverage, but for this study, we have selected a subdomain covering Scandinavia, from 53° to 72° latitude and between 0° and 32° longitude. The border of the selected ERA5 spatial subdomain is indicated with a blue line in Fig. 2 a). The selected 5-year time period for this study is from 1 January 2015 to 31 December 2019.

2.4. NORA3 mesoscale data

NORA3, the 3-km Norwegian Reanalysis, is a mesoscale atmospheric hindcast dataset for the Norwegian Sea, the North, and the Barents Sea, currently covering the time period from 1969 to 2023 [24]. It is dynamically downscaled from ERA5 reanalysis using the HARMONIE-AROME model, providing atmospheric fields on a 3-km spatial resolution. NORA3 includes a convection-permitting non-hydrostatic model that resolves mesoscale features, thus it is expected to provide superior performance on precipitation compared to ERA5. A one-hour time resolution is achieved by deterministic forecasts every 6 hours with lead times from 3 to 9 hours for near-surface parameters. The 3-hour lead time output serves as a reference for the conversion of accumulated parameters, which are summed up from the start of each forecast. For a good overlap with ERA5 for the area of interest, we limit our analyses to a subdomain of NORA3 spanned by 57.72°N, -16.47°E; 48.02°N,6.97°E; 59.87°N, 42.41°E; and 76.30°N, 26.33°E: In this study, we make use of the 1h-mean horizontal wind speed at an assumed hub height of 150 m, interpolated from the nearest available output levels at 100 m and 250 m, and the accumulated precipitation parameters. To achieve the highest level of comparability between ERA5 and NORA3 we decided to focus on liquid precipitation only. Thus we compute the mean-hourly rain rate as the difference between the total accumulated precipitation amount (NORA3 parameter: *precipitation_amount_acc*) and the total accumulated solid precipitation (*snowfall_amount_acc*) minus the corresponding value from the previous lead time.

2.5. Weather station data at two selected sites

Observations from two coastal weather stations, Thyborøn in Denmark and Utsira Fyr in Norway (Fig. 2 b), are used for comparison to the ERA5 and NORA3 data for wind speed and rainfall. These two sites were selected since the corresponding data sets of precipitation and wind observations are sufficiently long and have a high enough time resolution for a model evaluation. Furthermore, they represent two separate sites that can be considered as representative of coastal and offshore conditions in suspectedly erosion-prone areas. The Utsira data covers a period from 2016-03-15 to 2019-03-15 while the Thyborøn time series is longer, from 2015-01-01 to 2019-12-31. Both weather station datasets have a 10-minute temporal resolution and the measurement height is 10 m for wind speed.

We calculate the power spectral density of the wind speed and rainfall intensity to analyze the variability at different frequencies. The spectral density of a measured time series (x) is estimated by

$$S_x(f) = \frac{1}{N f_s} |\hat{x}|^2 \tag{4}$$

where f is the frequency, f_s is the sampling frequency, N is the number of measurements in the time series, and $\hat{x}$ is the discrete Fourier transform of x.

[1] the vertical velocity component of the droplets is averaged out during the time step due to the rotation of the blade.

Table 2
Statistics and rain erosion damage model results at the weather stations Utsira and Thyborøn based on measured data, ERA5 and NORA3. The relative differences to the observations are given in parentheses. The average wind speed values from the measurements are extrapolated to the 150 m-level (marked with an asterisk).

#	Weather station	Data source	Average wind speed [m/s]	Average annual rainfall [mm]	Average annual impinged water [m]	Erosion onset time [years]
A	Utsira	Meas.	9.58*	1319	22.32	2.49
		ERA5	9.33 (−2.6%)	1626 (+23.3%)	34.53 (+54.7%)	1.69 (−32.1%)
		NORA3	9.57 (−0.1%)	1240 (−6.0%)	23.63 (+5.9%)	2.34 (−5.8%)
B	Thyborøn	Meas.	8.44*	843	12.89	6.48
		ERA5	9.40 (+11.3%)	964 (+14.4%)	20.97 (+62.8%)	3.04 (−53.0%)
		NORA3	9.68 (+14.7%)	870 (+3.2%)	17.17 (+33.3%)	3.44 (−46.9%)

As the damage model uses hub height wind speed as an input, we use extrapolated 10 m wind speeds for the comparison with the modeled data. The extrapolation is done to 150 m with the power law:

$$U(z) = U_{ref}\left(\frac{z}{z_{ref}}\right)^{\alpha} \tag{5}$$

where U_{ref} and z_{ref} are the reference wind speed and height (10 m) respectively and α is the shear exponent. Note that there is a considerable uncertainty involved with vertical extrapolation of this kind, due to changes in the shear exponent with time, height, wind direction, and atmospheric stability. However, we choose this approach for simplicity. For the Utsira wind data, we use $\alpha = 0.063$ based on Peña et al. [28] where the shear exponent has been estimated at Utsira. To the authors' knowledge, the shear exponent has not been estimated at Thyborøn, so we use an estimate of $\alpha = 0.077$ from Høvsøre [29] which is a nearby site. More details about the weather station data can be found in Hasager et al. [12].

3. Results

3.1. Analysis of data at two weather station sites

In this section, we compare the measured wind speed and rainfall data with the modeled data and the calculated damages at the two weather stations Utsira and Thyborøn. The model data time series are selected from the nearest grid points of the two sites.

The smoothed power spectral density of the time series can be seen in Fig. 3. The smoothing is done so that 15 estimates appear in each decade, mainly smoothing the spectrum in the high-frequency range. Here it can be noticed that the measured time series extend to higher frequencies than both models due to the higher temporal resolution of the measured data. The spectral slope of the measured wind speed and NORA3 wind speed is close to the theoretical slope in the inertial range of $f^{-5/3}$ for frequencies above $2\,\mathrm{day}^{-1}$ (Fig. 3 a) and b)). For comparison, the ERA5 wind speed spectra have a much steeper slope due to the lower spatial resolution of the data. Note that a grid cell covers a $3 \times 3\,\mathrm{km}^2$ in NORA3, whereas in ERA5 a grid cell corresponds to an area of approximately $30 \times 13\,\mathrm{km}^2$.

Similarly, we see in Fig. 3 c) and d) that the rain intensity spectra for ERA5 have a higher spectral slope in the high-frequency range. The spectral slope of the NORA3 rain intensity follows the slope of the measurements better, especially at Thyborøn (Fig. 3 d)).

Table 2 shows the annual average wind speed at 150 m height and average annual rainfall at the weather stations and the corresponding nearest grid cell in ERA5 and NORA3. The calculated mean annual values of impinged water and erosion onset time are listed as well as the relative difference to the measured data. Note that for Utsira, the period covered is from 2016-03-15 to 2019-03-15, and for Thyborøn from 2015-01-01 to 2019-12-31. The period is limited by available weather station measurements from met.no and DMI for direct comparison between models and measurements.

The comparison of wind speeds at the coastal station Utsira shows good agreement of both reanalysis products to the vertically extrapolated wind speed from the observations, with ERA5 wind speed being slightly lower (Table 2). At Thyborøn, both models have a larger positive wind speed bias compared to the observations. However, here it should be noted that the wind speed measurements at Thyborøn are influenced by nearby buildings that give an increased roughness and reduced wind speeds for some periods, resulting in data values at and close to 0 m/s.

At Utsira, the average annual measured rainfall is much closer to NORA3 than to ERA5 with a relative bias of −6% and +23%, respectively. At Thyborøn, the picture is similar, with both NORA3 (+3%) and ERA5 (+14%) showing positive deviations.

For the average annual impinged water and erosion onset time, both resulting from the wind speed and rainfall data, both models indicate a higher amount of impinged water for both locations and correspondingly earlier erosion onset times compared to the measurements. In general, NORA3 shows a better agreement with the reference and the spread between the models is much larger at Utsira than at Thyborøn, with ERA5 indicating the onset of erosion already after 1.7 years at Utsira. The earlier onset time at Utsira from NORA3 may, at first sight, appear counterintuitive, since the annual rainfall is less compared to the observations, whereas the average wind speeds are almost identical. In this case, the resulting values are caused by a higher correlation between rain events and periods of high wind speeds in NORA3 than in the measurements.

Fig. 4 shows the cumulative rain at Utsira (a) and Thyborøn (b) and the corresponding modeled damage increments (c and d). Comparing the measured rain with NORA3 we see that for some periods the rain is underestimated and other periods overestimated, but the final cumulative rainfall is comparable. ERA5 rainfall is overestimated more regularly. At Utsira the picture for the cumulative damage increments is similar with a much better agreement between the observations and NORA3 (Fig. 4 c)). However, at Thyborøn both models agree better in terms of the cumulative damage increments, with clearly higher values than the observations (Fig. 4 d)). Parts of this behavior can be attributed to the wind speed measurements not being representative during all times as mentioned above.

3.2. Rain Erosion Atlas Layers based on ERA5 and NORA3

Fig. 5 shows the annual mean rainfall from ERA5 data a) and from NORA3 b) and the mean wind speed at 150 m height.

When comparing the ERA5 layers with NORA3 we see greater details in both wind and rain fields, especially in the mountain areas. The area experiencing the highest amount of annual precipitation lies on the west coast of Norway. For ERA5 this area extends offshore, while for the NORA3 rain, it is confined onshore along the coast. The mean wind speed over land in complex terrain is known to be underestimated in ERA5 [24], likely due to enhanced surface roughness, and we can clearly see this for the mean wind field at 150 m when comparing Fig. 5 c) and d). The ERA5 mean wind speeds over Norway are the lowest wind speeds on the whole map, while in NORA3 the wind speeds in the same area show some distinct peaks due to speedup effects over the mountains.

The annual accumulated impinged water/rainfall of the IEA 15 MW wind turbine can be seen in Fig. 6 based on ERA5 data in a) and based

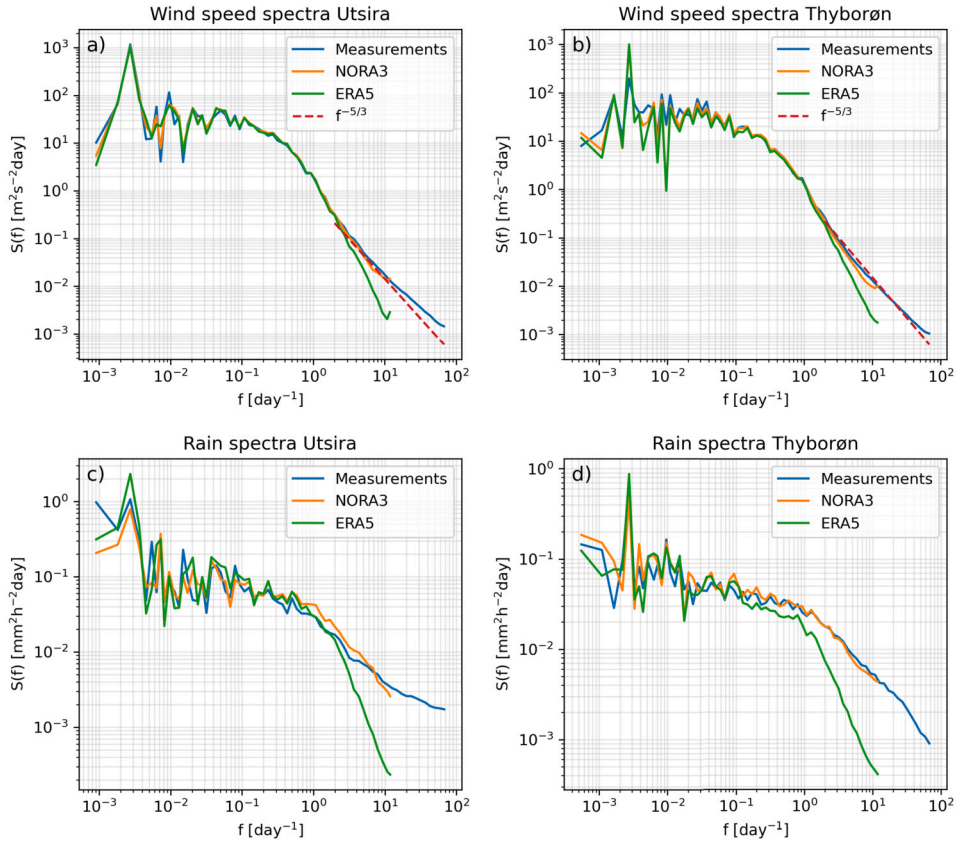

Fig. 3. Wind speed and rainfall intensity power spectrum comparing measurement, NORA3 and ERA5 at Utsira (Norway) and Thyborøn (Denmark). The theoretical spectral slope line $f^{-5/3}$ is shown for higher frequency wind speed.

on NORA3 data in b). We see that the highest values of impinged water on the map can reach 40 m and above. The amount of impinged water that the tip of the blade will encounter in a year depends on the wind speed, rainfall, and wind turbine tip speed (of the assumed wind turbine model), but is independent of the blade material. However, for the onset time of erosion, the impinged water amount has been coupled with the VH curve of a commercial blade material. Fig. 6 c) and d) show the onset time of erosion for the IEA 15 MW wind turbine with the assumed commercial material based on ERA5 and NORA3 data, respectively. The maximum onset time of the color scale is limited to 25 years, which is a typical lifetime of wind turbine components.

We see that the offshore areas have the highest amount of accumulated impinged water and the shortest onset time of erosion. The main difference between the erosion onset time for NORA3 and ERA5 are that the short onset times extend further inland in Norway for the NORA3 data, due to the higher amount of modeled rainfall and higher wind speed on the west coast of Norway.

3.3. Focus on offshore areas

Fig. 7 shows the onset time of rain erosion where the land areas have been masked out and the color scale is limited to 5 years. This is done to have a better view of the variation in incubation time over the offshore areas. Comparing the prediction based on ERA5 a) to NORA3 b), it can be seen that the predicted erosion onset time is shortest along the westward coastal lines for the ERA5 dataset. This coastal effect can not be seen in the erosion onset time based on the NORA3 dataset and the predicted damage onset are generally at later times for the offshore areas in NORA3.

Table 3 lists the values of the different atlas layers (Fig. 5 and Fig. 6) extracted at wind farm sites in the Norwegian and the North Seas (henceforth called North Sea). The location and the numbering of the wind farm sites can be seen in Fig. 2 b). The results are based on model data of the time period from 01.01.2015 to 31.12.2019 (5 years). It is shown in section 3.1 that NORA3 is closer to the measured rainfall than ERA5. Thus, to be consistent with the calculation of the relative bias, we choose to normalize with NORA3.

The average wind speeds at the North Sea offshore sites are 10.2 m/s in ERA5 and 10.3 m/s in NORA3. For offshore sites, the average relative bias in wind speeds is minimal with -0.6%, i.e., the wind speed in NORA3 is slightly higher than in ERA5 at 150 m. The only exception is the inland site Bergen, which has a lower wind speed (≈6.3 m/s) than the offshore sites.

The average annual rainfall at the North Sea sites has a relative bias of 19.8%. ERA5 estimates higher average annual rainfall (1004 mm) than NORA3 (839 mm). On average, ERA5 is 165 mm wetter than NORA3. ERA5 shows a positive bias at all sites. Both models indicate the highest rainfall at the northernmost offshore site and the lowest rainfall at the southernmost offshore site. In Bergen, located inland, the average annual rainfall in both models is very high (>2200 mm).

Results for the six offshore wind farm sites in the Inner Danish and Baltic Seas (henceforth called Baltic Sea) are listed in Table 4. Average wind speeds in ERA5 (9.4 m/s) and NORA3 (9.5 m/s) compare well with a relative bias of −0.9%. At EnBW Baltic, an absolute difference of 0.7 m/s (relative bias −7.2%) is noted. The average annual rainfall in ERA5 (715 mm) is larger than in NORA3 (622 mm). ERA5 is, on average, 93 mm wetter than NORA3 (relative bias of 15.0%).

In summary, ERA5 and NORA3 compare well for wind speeds data in the Baltic Sea, while ERA5 shows higher precipitation levels than NORA3. The Baltic Sea is characterized by lower wind speeds and lesser rainfall than the North Sea. Consequently, the average onset time for erosion at wind farm sites in the Baltic Sea is longer. Based on NORA 3, erosion onset time is estimated to be 5 years in Baltic Sea locations and 3.2 years in North Sea sites.

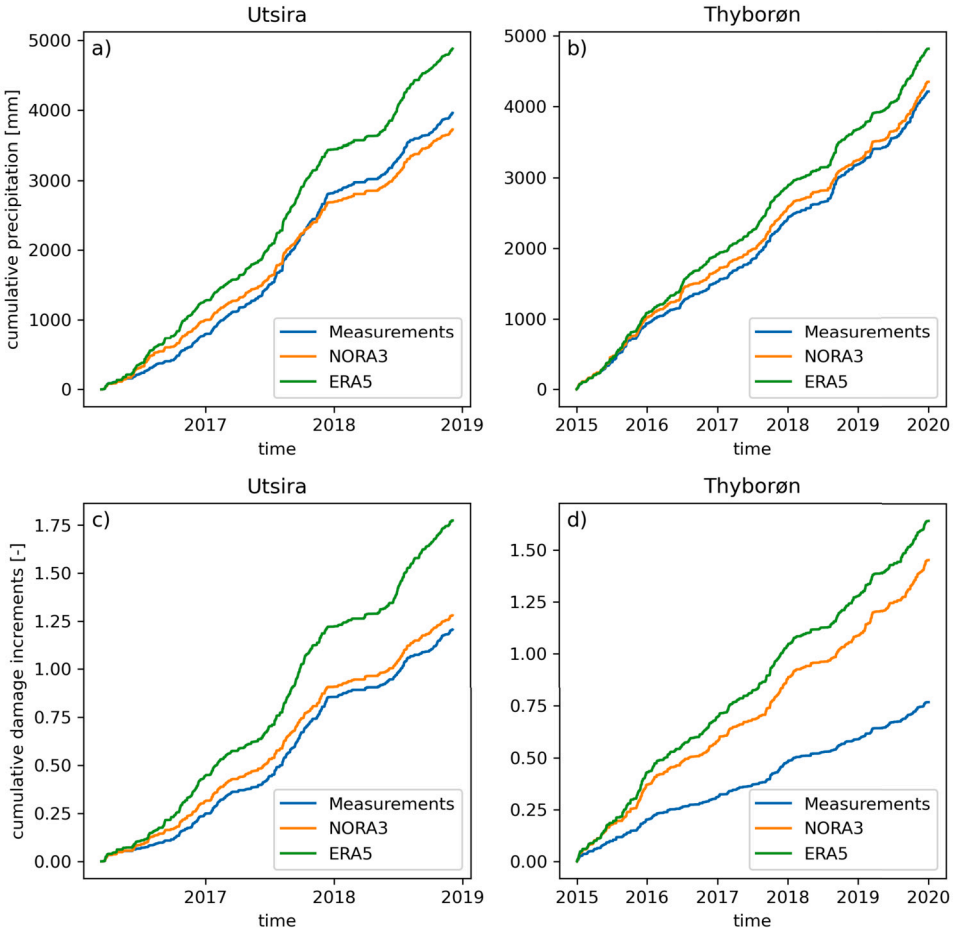

Fig. 4. Cumulative rainfall comparing measurement, NORA3 and ERA5 at Utsira (Norway) and Thyborøn (Denmark). The time period is matched with the available measurements.

Table 3
Average wind speed at 150 m, annual average rainfall and impinged water, and erosion onset time at North Sea sites (see Fig. 5), based on ERA5 and NORA3, and for the IEA 15 MW wind turbine with a commercial blade coating.

#	Wind farm site	Data source	Average wind speed [m/s]	Average annual rainfall [mm]	Average annual impinged water [m]	Erosion onset time [years]
1	Hywind Tampen	ERA5	10.2	1342	29.8	1.8
		NORA3	10.6	1151	23.3	2.2
2	Bergen Florida	ERA5	5.9	2548	45.1	2.1
		NORA3	6.7	2209	38.3	1.8
3	Sørlige Nordsjø II	ERA5	10.5	935	21.8	2.5
		NORA3	10.6	799	16.6	3.1
4	Thor	ERA5	10.4	967	22.4	2.5
		NORA3	10.3	806	16.6	3.3
5	Horns Rev II	ERA5	10.2	901	21.0	2.7
		NORA3	10.2	765	15.9	3.4
6	Dan Tysk	ERA5	10.2	939	21.8	2.6
		NORA3	10.2	765	15.9	3.4
7	Alpha Ventus	ERA5	9.9	942	22.1	2.6
		NORA3	9.9	745	15.2	3.7
	Offshore Averages	**ERA5**	10.2	1004	23.2	2.4
		NORA3	10.3	839	17.2	3.2
		Rel. bias	−0.6%	19.8%	34.3%	−23.5%

Offshore regions are here generally identified as critical areas for rain erosion. For a turbine of a similar size of the IEA 15 MW, the commercial blade material coating assessed in this study would start to erode within the first quarter of the expected turbine lifetime. We observe that there is a considerable variation in predicted erosion onset times in the offshore areas. Wind farm locations in the Baltic Sea and inner Danish seas exhibit significantly longer erosion onset times compared to those in the North Sea. Furthermore, the maps in Fig. 7 highlight the offshore areas along the southwest coast of Norway as the most critical regions for rain erosion.

4. Discussion

Our study presents a complete rain erosion atlas for wind turbine blades in Scandinavia and adjacent offshore regions. As this is the first

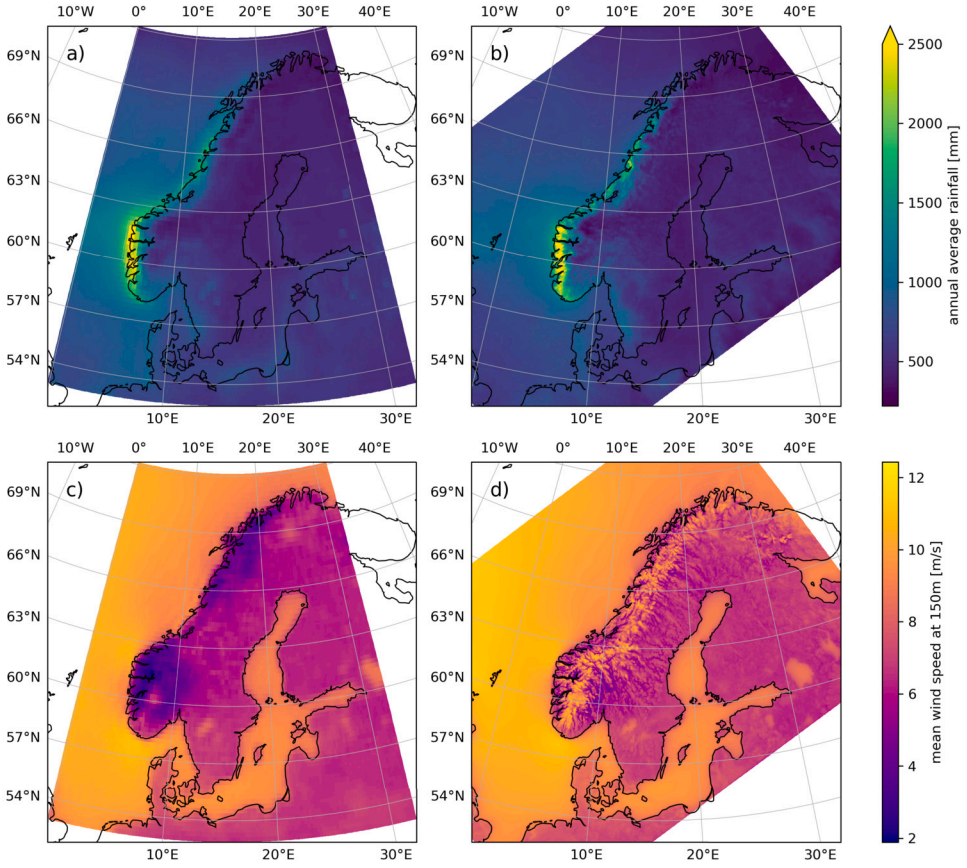

Fig. 5. The annual average rainfall for a) ERA5, b) NORA3 and average wind speed at 150 m for c) ERA5 and d) NORA3.

Table 4
Average wind speed at 150 m, annual average rainfall and impinged water, and erosion onset time at Baltic Sea sites (see Fig. 5), based on ERA5 and NORA3, and for the IEA 15 MW wind turbine with a commercial blade coating.

#	Wind farm site	Data source	Average wind speed [m/s]	Average annual rainfall [mm]	Average annual impinged water [m]	Erosion onset time [years]
8	Anholt	ERA5	9.6	761	17.6	3.4
		NORA3	9.6	678	13.7	4.4
9	Vindeby	ERA5	9.5	727	16.5	3.8
		NORA3	9.1	662	13.1	5.0
10	Rødsand II	ERA5	9.1	761	17.2	3.7
		NORA3	9.4	646	12.8	5.0
11	Kriegers Flak	ERA5	9.7	691	16.0	3.8
		NORA3	9.6	576	11.8	5.3
12	EnBW Baltic	ERA5	8.7	663	14.7	4.8
		NORA3	9.4	589	12.0	5.2
13	Bornholm	ERA5	9.7	689	15.8	3.9
		NORA3	9.7	580	11.7	5.2
	Offshore	**ERA5**	9.4	715	16.3	3.9
	Averages	**NORA3**	9.5	622	12.5	5.0
		Rel. bias	−0.9%	15.0%	30.3%	−21.9%

of its kind, there are no existing maps to directly compare the general patterns of the erosion onset time results. Nonetheless, related research [17,7,11,13] has been conducted on blade coating lifetimes and incubation periods in specific locations also covered by our atlas. These studies consistently indicate that the predicted lifetimes or incubation periods tend to be shorter in coastal and offshore regions, aligning with the findings of our research.

Our comparative analysis with actual measurements indicates that the NORA3 rain field predictions align more accurately with observed rainfall than those from ERA5 at both measurement sites. This is evident both in the frequency domain (as shown in Fig. 3) and in terms of cumulative rainfall (illustrated in Fig. 4). This finding is consistent with prior research [30–33] identifying a wet bias in the ERA5 rainfall. The relative lack of high-frequency energy content in ERA5 rain predictions, coupled with its overall higher cumulative rainfall, leads to a temporal 'smearing' of rain events in the model, resulting in more frequent but less intense rain events.

The discrepancies between the rain predictions of these models significantly influence the modeled damage progression (as depicted in Fig. 4). It is observed that the cumulative damage progression generally mirrors the pattern of cumulative rainfall. However, there is a notable exception in the damage progression based on measurements at Thyborøn (Fig. 4 d)), which stands out as an anomaly, due to the differences in wind speed. The measured wind speeds at Thyborøn are affected by

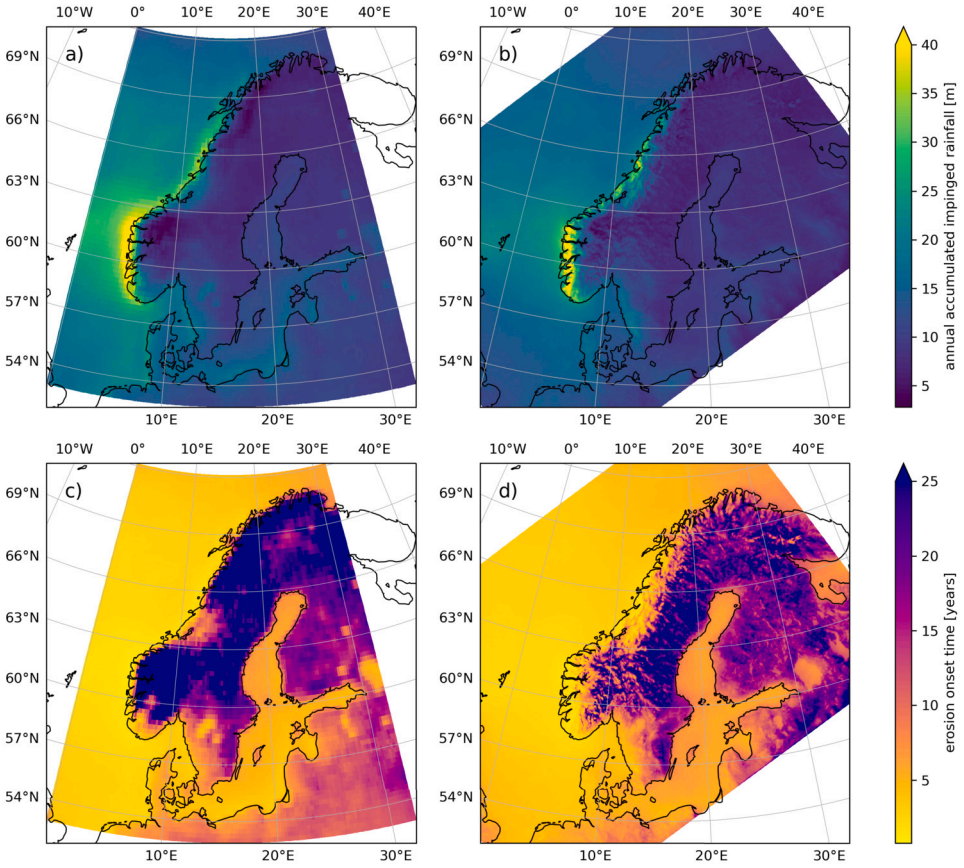

Fig. 6. The annual accumulated impinged rainfall for a) ERA5, b) NORA3 and the onset time of erosion for c) ERA5 and d) NORA3. The layers are calculated for the IEA 15 MW wind turbine (all panels) and a commercial blade material (lower panels).

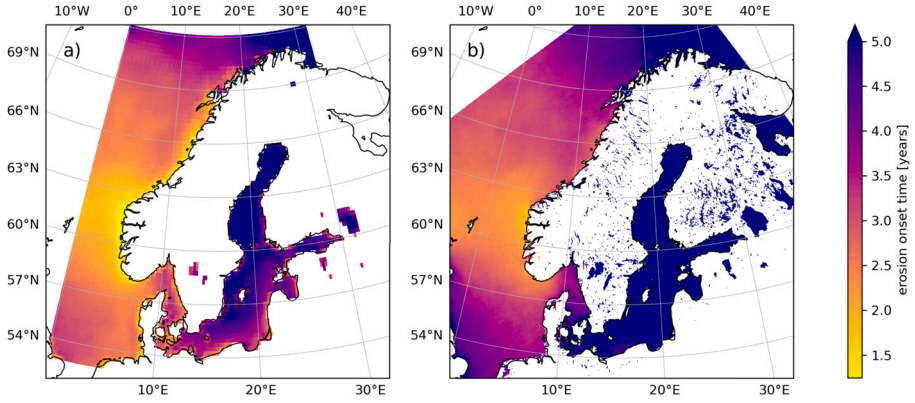

Fig. 7. The onset time of rain erosion for a) ERA5 and b) NORA3 for sea areas. The layers are calculated for the IEA 15 MW wind turbine and a commercial blade material.

nearby structures and obstacles, and although these speeds have been extrapolated using the power law, they occasionally approach 0 m/s. In contrast, the modeled wind speeds are not influenced by these obstacles and are therefore higher on average and do not include prolonged periods below the cut-in wind speed of the reference wind turbine.

The maps of annual average wind speed in Fig. 2 show a notable difference between the modeled wind speed in the mountainous area of Norway, where the ERA5 wind speed is significantly lower. This difference aligns with a number of studies that have shown that the ERA5 wind speed is underestimated in mountainous terrain [24,34,35]. Several factors likely contribute to the underestimation of ERA5 wind speeds in mountainous terrain. Firstly, the low spatial resolution of ERA5 is insufficient to model the acceleration of winds over hill- and mountain tops, i.e. the orographic speed up effect is under-resolved. Secondly, the representation of orographic drag processes, recognized as a significant source of uncertainty in numerical weather prediction models [36], leads to too high drag over mountainous areas in ERA5. Lastly, the hydrostatic model formulation of ERA5 neglects vertical acceleration, which limits the simulated wind flow over the mountains. This differs from the non-hydrostatic dynamics used in NORA3.

Given the well-established tendency of ERA5 to underestimate wind speeds onshore, particularly in complex terrain [24,34,35], a notable difference was expected between the erosion layer results of NORA3 and ERA5 in the onshore areas. Conversely, the results for offshore areas were expected to be more aligned. This expectation is largely confirmed in our findings, as illustrated in Fig. 6 and Fig. 7, where the offshore

results are indeed more consistent. However, it's noteworthy that the incubation times in these offshore areas are significantly lower for the predictions based on ERA5, as detailed in Tables 2 and 3. The primary reason for this discrepancy appears to be the wet bias present in the ERA5 dataset since the mean offshore winds from both models are more similar (low relative bias in Tables 2 and 3).

In the erosion onset time map derived from ERA5 data (Fig. 6 c), we observe a pronounced increase in erosion risk along the western coasts, indicated by shorter incubation times. This pattern is likely a consequence of the limited spatial resolution of the ERA5 model, which does not adequately resolve coastal features. As a result, the influence of the coastline, such as changes in surface roughness and elevation, is overextended into offshore areas, impacting both wind fields and precipitation patterns. In contrast, the NORA3 rain erosion map (Fig. 6 d) reveals that the highest erosion risk is located inland on the west coast of Norway. Despite NORA3 being a modeled dataset with its own set of errors, the substantially higher spatial resolution provides more reliable results, as elaborated in Section 2.4.

The damage model employed in our atlas is founded on rain erosion tests and is specifically designed to predict the onset of erosion due to liquid precipitation only. This means our results exclusively consider erosion due to rain, without accounting for other erosive factors like hail, wet snow, UV radiation, and sandstorms [1]. Nevertheless, within the scope of our study, which focuses on Scandinavia, rain is presumed to be the predominant factor contributing to leading-edge erosion damages, although further research may be needed to conclusively confirm this assumption.

Unlike a wind atlas, a rain erosion atlas is essentially linked to specific wind turbine characteristics. A wind atlas is based on wind data and the wind resource and energy density are calculated without information about a specific wind turbine. Thus energy density is a turbine-agnostic metric. In contrast, rain erosion is related to the impinged water at the specific blade. Thus, the rain erosion atlas is valid for specific turbine parameters with the key information of the blade tip speed. To predict the damage progression and blade lifetime, it is necessary to have information on the VH curve from the rain erosion test for the specific coating material. Using a VH curve for a more durable coating material would lead to longer erosion onset times for our results. We would also increase the incubation times by using reference turbine models for smaller turbines, e.g. a 10 MW or a 5 MW turbines that operate at lower heights with lower speeds and have shorter blades leading to lower maximum tip speeds. It should also be noted that the onset time of erosion only marks the initial signs of erosion, differing from the overall blade lifetime which indicates a more severe stage of erosion requiring blade repair. Therefore, repair interventions would occur significantly later than the initial onset of erosion.

5. Conclusion

In this study, we have demonstrated a framework that can effectively identify areas prone to erosion due to liquid precipitation. This marks the first creation of a rain erosion atlas for the Scandinavian region including Denmark and Finland. We compared the results derived from ERA5 and NORA3 with those derived from weather station measurements at Utsira in Norway and Thyborøn in Denmark. It is evident that NORA3 data correspond more closely with the actual measurements across various parameters, including power spectral density, mean wind speed, annual accumulated rainfall, and the predicted rain erosion damage.

The findings from the Scandinavian rain erosion atlas can be summarized as follows:

- Areas characterized by high precipitation combined with high wind speed exhibit shorter erosion onset times;
- Offshore areas are identified as critical for rain erosion, with the southwest coast of Norway being the most critical area;
- Results at selected wind farm location in the North Sea, the onset time of erosion is on average 3.2 years and 5 years in the Baltic sea, based on NORA3 data;
- Based on NORA3 data, the onset time of erosion is on average 5 years for Baltic Sea wind farm sites and 3.2 years for North Sea sites

Our findings reveal that the ERA5 model overestimates rain at all analyzed wind farm locations with a relative bias of 20% at North Sea and Norwegian Sea locations and 15% at the inner Danish Seas and Baltic Sea. The wind speed bias is generally low, less than -1%. This discrepancy leads to an underestimation of the onset time of erosion based on ERA5, where the relative bias is -24% at North Sea and Norwegian Sea locations and -22% at the inner Danish Seas and Baltic Sea.

Our research highlights the importance of considering both wind and rain parameters in assessing erosion risk. The differences in model performance underscore the need for utilizing high-resolution data, like that from NORA3, for more accurate predictions, especially in coastal and offshore areas. This study lays the groundwork for future research in this field and offers valuable insights for the wind energy sector, particularly in optimizing turbine design and maintenance strategies in erosion-prone regions.

CRediT authorship contribution statement

Ásta Hannesdóttir: Writing – original draft, Writing – review & editing, Visualization, Validation, Software, Methodology, Investigation, Funding acquisition, Formal analysis, Data curation, Conceptualization. **Stephan T. Kral:** Writing – original draft, Writing – review & editing, Visualization, Validation, Software, Methodology, Investigation, Data curation, Conceptualization. **Joachim Reuder:** Writing – original draft, Writing – review & editing, Methodology, Investigation, Funding acquisition, Conceptualization. **Charlotte Bay Hasager:** Writing – original draft, Writing – review & editing, Investigation, Funding acquisition, Formal analysis, Conceptualization.

Declaration of competing interest

The authors confirm that there are no competing financial interests or personal relationships that might be perceived to have influenced the findings presented in this paper.

Data availability

The python code used to calculate the atlas layers, data with calculated atlas layers, and a python script for plotting is available at: https://gitlab.windenergy.dtu.dk/astah/era5_erosion_atlas.

Acknowledgement

This research was supported by the project "Estimation and Prevention of Erosion on Off-Shore Wind Turbine Blades" (102235103) funded by the Academia Agreement between the University of Bergen and Equinor. Authors Hannesdóttir and Hasager acknowledge the partial support of the IEA task 46 "Erosion of wind turbine blades" EUDP grant J.nr. 64021-0003 and the project HORIZON Europe Grant "AIRE" (101083716).

We acknowledge the ECMWF for the ERA5 data, the Norwegian Meteorological Institute for the Utsira Fyr measurements and the NORA3 data, and the Danish Meteorological Institute for the measurements at Thyborøn.

References

[1] W. Han, J. Kim, B. Kim, Effects of contamination and erosion at the leading edge of blade tip airfoils on the annual energy production of wind turbines, Renew. Energy 115 (2018) 817–823, https://doi.org/10.1016/j.renene.2017.09.002.

[2] M.H. Keegan, D.H. Nash, M.M. Stack, On erosion issues associated with the leading edge of wind turbine blades, J. Phys. D, Appl. Phys. 46 (38) (2013) 383001, https://doi.org/10.1088/0022-3727/46/38/383001.
[3] L. Mishnaevsky, K. Thomsen, Costs of repair of wind turbine blades: influence of technology aspects, Wind Energy 23 (12) (2020) 2247–2255, https://doi.org/10.1002/we.2552.
[4] L. Mishnaevsky, C.B. Hasager, C. Bak, A.M. Tilg, J.I. Bech, S. Doagou Rad, S. Fæster, Leading edge erosion of wind turbine blades: understanding, prevention and protection, Renew. Energy 169 (2021) 953–969, https://doi.org/10.1016/j.renene.2021.01.044.
[5] S.C. Pryor, R.J. Barthelmie, J. Cadence, E. Dellwik, C.B. Hasager, S.T. Kral, J. Reuder, M. Rodgers, M. Veraart, Atmospheric drivers of wind turbine blade leading edge erosion: review and recommendations for future research, Energies 15 (22) (2022) 8553, https://doi.org/10.3390/en15228553.
[6] DNVGL-RP-0171, Testing of Rotor Blade Erosion Protection Systems, Recommended practice, DNV GL, Oslo, Norway (2018).
[7] J.I. Bech, N.F.J. Johansen, M.B. Madsen, Á. Hannesdóttir, C.B. Hasager, Experimental study on the effect of drop size in rain erosion test and on lifetime prediction of wind turbine blades, Renew. Energy 197 (2022) 776–789, https://doi.org/10.1016/j.renene.2022.06.127.
[8] R. Prieto, T. Karlsson, A model to estimate the effect of variables causing erosion in wind turbine blades, Wind Energy 24 (9) (2021) 1031–1044, https://doi.org/10.1002/we.2615.
[9] J. Visbech, T. Göçmen, C.B. Hasager, H. Shkalov, M. Handberg, K.P. Nielsen, Introducing a data-driven approach to predict site-specific leading-edge erosion from mesoscale weather simulations, Wind Energy Sci. 8 (2) (2023) 173–191, https://doi.org/10.5194/wes-8-173-2023.
[10] D. Eisenberg, S. Laustsen, J. Stege, Wind turbine blade coating leading edge rain erosion model: development and validation, Wind Energy 21 (10) (2018) 942–951, https://doi.org/10.1002/we.2200.
[11] C. Hasager, F. Vejen, J.I. Bech, W.R. Skrzypiński, A.M. Tilg, M. Nielsen, Assessment of the rain and wind climate with focus on wind turbine blade leading edge erosion rate and expected lifetime in Danish Seas, Renew. Energy 149 (2020) 91–102, https://doi.org/10.1016/j.renene.2019.12.043.
[12] C.B. Hasager, F. Vejen, W.R. Skrzypiński, A.-M. Tilg, Rain erosion load and its effect on leading-edge lifetime and potential of erosion-safe mode at wind turbines in the North Sea and Baltic Sea, Energies 14 (7) (2021) 1959, https://doi.org/10.3390/en14071959.
[13] A.S. Verma, Z. Jiang, M. Caboni, H. Verhoef, H. van der Mijle Meijer, S.G. Castro, J.J. Teuwen, A probabilistic rainfall model to estimate the leading-edge lifetime of wind turbine blade coating system, Renew. Energy 178 (2021) 1435–1455, https://doi.org/10.1016/j.renene.2021.06.122.
[14] A.S. Verma, Z. Jiang, Z. Ren, M. Caboni, H. Verhoef, H. Mijle-Meijer, S.G. Castro, J.J. Teuwen, A probabilistic long-term framework for site-specific erosion analysis of wind turbine blades: a case study of 31 Dutch sites, Wind Energy 24 (11) (2021) 1315–1336, https://doi.org/10.1002/we.2634.
[15] F. Letson, R.J. Barthelmie, S.C. Pryor, Radar-derived precipitation climatology for wind turbine blade leading edge erosion, Wind Energy Sci. 5 (1) (2020) 331–347, https://doi.org/10.5194/wes-5-331-2020.
[16] H. Punge, K. Bedka, M. Kunz, A. Reinbold, Hail frequency estimation across Europe based on a combination of overshooting top detections and the ERA-INTERIM reanalysis, Atmos. Res. 198 (June 2017) 34–43, https://doi.org/10.1016/j.atmosres.2017.07.025.
[17] M. Badger, H. Zuo, Á. Hannesdóttir, A. Owda, C. Hasager, Lifetime prediction of turbine blades using global precipitation products from satellites, Wind Energy Sci. 7 (6) (2022) 2497–2512, https://doi.org/10.5194/wes-7-2497-2022.
[18] N. Mortensen, J. Hansen, M. Kelly, E. Prinsloo, E. Mabille, S. Szewczuk, Wind Atlas for South Africa (WASA) Station and Site Description Report, 2012.
[19] N. Nawri, G. Petersen, H. Björnsson, A. Hahmann, K. Jónasson, C. Hasager, N.-E. Clausen, The wind energy potential of Iceland, Renew. Energy 69 (2014) 290–299, https://doi.org/10.1016/j.renene.2014.03.040, this is an open access article under the CC BY-NC-ND license.
[20] A.N. Hahmann, T. Sīle, B. Witha, N.N. Davis, M. Dörenkämper, Y. Ezber, E. García-Bustamante, J.F. González-Rouco, J. Navarro, B.T. Olsen, S. Söderberg, The making of the new European wind atlas – Part 1: model sensitivity, Geosci. Model Dev. 13 (10) (2020) 5053–5078, https://doi.org/10.5194/gmd-13-5053-2020, https://gmd.copernicus.org/articles/13/5053/2020/.
[21] N. Davis, J. Badger, A. Hahmann, B. Hansen, N. Mortensen, M. Kelly, X. Larsén, B. Olsen, R. Floors, G. Lizcano, P. Casso, O. Lacave, A. Bosch, I. Bauwens, O. Knight, A. Loon, R. Fox, T. Parvanyan, S. Hansen, D. Heathfield, M. Onninen, R. Drummond, The global wind atlas: a high-resolution dataset of climatologies and associated web-based application, Bull. Am. Meteorol. Soc. 104 (8) (2023) E1507–E1525, https://doi.org/10.1175/BAMS-D-21-0075.1.
[22] X.G. Larsén, N. Davis, Á. Hannesdóttir, M. Kelly, L. Svenningsen, R. Slot, M. Imberger, B.T. Olsen, R. Floors, The global atlas for siting parameters project: extreme wind, turbulence, and turbine classes, Wind Energy 25 (11) (2022) 1841–1859, https://doi.org/10.1002/we.2771, https://onlinelibrary.wiley.com/doi/pdf/10.1002/we.2771, https://onlinelibrary.wiley.com/doi/abs/10.1002/we.2771.
[23] H. Hersbach, B. Bell, P. Berrisford, S. Hirahara, A. Horányi, J. Muñoz-Sabater, J. Nicolas, C. Peubey, R. Radu, D. Schepers, A. Simmons, C. Soci, S. Abdalla, X. Abellan, G. Balsamo, P. Bechtold, G. Biavati, J. Bidlot, M. Bonavita, G. Chiara, P. Dahlgren, D. Dee, M. Diamantakis, R. Dragani, J. Flemming, R. Forbes, M. Fuentes, A. Geer, L. Haimberger, S. Healy, R.J. Hogan, E. Hólm, M. Janisková, S. Keeley, P. Laloyaux, P. Lopez, C. Lupu, G. Radnoti, P. Rosnay, I. Rozum, F. Vamborg, S. Villaume, J. Thépaut, The ERA5 global reanalysis, Q. J. R. Meteorol. Soc. 146 (730) (2020) 1999–2049, https://doi.org/10.1002/qj.3803.
[24] H. Haakenstad, Ø. Breivik, B.R. Furevik, M. Reistad, P. Bohlinger, O.J. Aarnes, NORA3: a nonhydrostatic high-resolution hindcast of the North Sea, the Norwegian Sea, and the Barents Sea, J. Appl. Meteorol. Climatol. 60 (10) (2021) 1443–1464, https://doi.org/10.1175/JAMC-D-21-0029.1.
[25] A.C. Best, The size distribution of raindrops, Q. J. R. Meteorol. Soc. 76 (327) (1950) 16–36, https://doi.org/10.1002/qj.49707632704.
[26] E. Gaertner, J. Rinker, L. Sethuraman, F. Zahle, B. Anderson, G. Barter, N. Abbas, F. Meng, P. Bortolotti, W. Skrzypinski, G. Scott, R. Feil, H. Bredmose, K. Dykes, M. Shields, C. Allen, A. Viselli, Definition of the IEA Wind 15-Megawatt Offshore Reference Wind Turbine, Technical Report, Tech. Rep., 2020.
[27] H. Slot, E. Gelinck, C. Rentrop, E. van der Heide, Leading edge erosion of coated wind turbine blades: review of coating life models, Renew. Energy 80 (2015) 837–848, https://doi.org/10.1016/j.renene.2015.02.036.
[28] A. Peña, T. Mikkelsen, S.-E. Gryning, C. Hasager, A. Hahmann, M. Badger, I. Karagali, M. Courtney, Offshore vertical wind shear: Final report on NORSEWInD's work task 3.11, no. 0005 in DTU Wind Energy E, DTU Wind Energy, Denmark, 2012.
[29] A. Peña, R. Floors, A. Sathe, S.-E. Gryning, R. Wagner, M. Courtney, X. Larsén, A. Hahmann, C. Hasager, Ten years of boundary-layer and wind-power meteorology at Høvsøre, Denmark, Bound.-Layer Meteorol. 158 (1) (2016) 1–26, https://doi.org/10.1007/s10546-015-0079-8.
[30] D.A. Lavers, A. Simmons, F. Vamborg, M.J. Rodwell, An evaluation of ERA5 precipitation for climate monitoring, Q. J. R. Meteorol. Soc. 148 (748) (2022) 3152–3165, https://doi.org/10.1002/qj.4351.
[31] Q. Jiang, W. Li, Z. Fan, X. He, W. Sun, S. Chen, J. Wen, J. Gao, J. Wang, Evaluation of the ERA5 reanalysis precipitation dataset over Chinese Mainland, J. Hydrol. 595 (10) (2021) 125660, https://doi.org/10.1016/j.jhydrol.2020.125660.
[32] D. Jiao, N. Xu, F. Yang, K. Xu, Evaluation of spatial-temporal variation performance of ERA5 precipitation data in China, Sci. Rep. 11 (1) (2021) 17956, https://doi.org/10.1038/s41598-021-97432-y.
[33] M. Bandhauer, F. Isotta, M. Lakatos, C. Lussana, L. Båserud, B. Izsák, O. Szentes, O.E. Tveito, C. Frei, Evaluation of daily precipitation analyses in E-OBS (v19.0e) and ERA5 by comparison to regional high-resolution datasets in European regions, Int. J. Climatol. 42 (2) (2022) 727–747, https://doi.org/10.1002/joc.7269.
[34] B. Jourdier, Evaluation of ERA5, MERRA-2, COSMO-REA6, NEWA and AROME to simulate wind power production over France, Adv. Appl. Sci. Res. 17 (2020) 63–77, https://doi.org/10.5194/asr-17-63-2020.
[35] M. Dörenkämper, B.T. Olsen, B. Witha, A.N. Hahmann, N.N. Davis, J. Barcons, Y. Ezber, E. García-Bustamante, J.F. González-Rouco, J. Navarro, M. Sastre-Marugán, T. Sīle, W. Trei, M. Žagar, J. Badger, J. Gottschall, J. Sanz Rodrigo, J. Mann, The making of the new European wind atlas – Part 2: production and evaluation, Geosci. Model Dev. 13 (10) (2020) 5079–5102, https://doi.org/10.5194/gmd-13-5079-2020, https://gmd.copernicus.org/articles/13/5079/2020/.
[36] I. Sandu, A. Zadra, N. Wedi, Impact of orographic drag on forecast skill (2017 2017), https://doi.org/10.21957/icghjblyn7, https://www.ecmwf.int/node/18163.